

Two new benzothiazine derivatives as corrosion inhibitors for mild steel in hydrochloric acid medium

K. Cherrak¹, A. Dafali^{1*}, A. Elyoussfi¹, Y. El Ouadi¹, N. K. Sebbar²,
M. El Azzouzi¹, H. Elmsellem¹, E. M. Essassi², A. Zarrouk¹

1. Laboratory of Applied Analytical Chemistry, Materials and Environment (URAC-18), Faculty of Sciences,
University of Mohammed Premier, B.P. 4808, 60046 Oujda, Morocco.

2. Laboratory of Heterocyclic Organic Chemistry, (URAC-21), Faculty of Sciences,
University of Mohammed V, B.P. 1014, Rabat, Morocco.

Received 18 Nov 2016,
Revised 13 Jan 2017,
Accepted 17 Jan 2017

Keywords

- ✓ Corrosion Inhibition
- ✓ Mild steel,
- ✓ Benzothiazine derivatives,
- ✓ Electrochemical techniques,
- ✓ HCl
- ✓ DFT

A. Dafali
E-mail: dafali2@yahoo.fr
+212 677 931 116

Abstract

The inhibition effects of 4-decyl-2H-benzo[b][1,4]thiazin-3(4H)-one (P1) and 2-benzylidene-4-decyl-2H-benzo[b][1,4]thiazin-3(4H)-one (P2) on mild steel corrosion in 1M HCl were studied in detail via gravimetric measurement, electrochemical impedance spectroscopy, potentiodynamic polarization and theoretical calculations. It was shown that P1 and P2 act were good corrosion inhibitors for mild steel protection. The inhibition efficiency of both the inhibitors increased with increasing concentration of inhibitor. Among them, P1 shows the highest inhibition efficiency of 97.7% at 10^{-3} M. The high inhibition efficiencies were attributed to the simple blocking effect by adsorption of inhibitor molecules on the steel surface. The inhibition action of the compound was assumed to occur via adsorption on the steel surface through the active centers in the molecule following Langmuir isotherm model. The relationship between inhibition efficiency and molecular structures of inhibitors was discussed using quantum chemical parameters.

1. Introduction

Mild steel is widely used in industrial applications. The acidic solutions are commonly used for the pickling, industrial acid cleaning, acid descaling, oil well acidifying, etc. Unfortunately, iron and its alloys could corrode during these acidic applications particularly with the use of hydrochloric acid, which results in terrible waste of both resources and money [1]. The decreasing of corrosion rate of metals provides saving of resources, economical benefits, increasing the lifetime of equipment and also decreasing the dissolution of toxic metals from the components into the environment [2]. Corrosion inhibitors are used to prevent metal dissolution [3-8]. Many research works have been developed in order to correlate the substituent effect and the inhibition efficiency of organic molecules [9,10]. The inhibition efficiency of organic compounds containing heterocyclic nitrogen increases with the number of aromatic rings and the availability of electronegative atoms in the molecule [11,12]. Quantum chemical calculations have been widely used to study reactional mechanisms and to interpret the experimental results as well as to resolve chemical ambiguities [13,14]. However, the inhibition efficiency was reinforced by the presence of heteroatoms such as sulfur, nitrogen and oxygen in the ring which facilitates its adsorption on metallic surface following the sequence $O < N < S$ [15-17].

The purpose of this paper is to investigate inhibition performance of 4-decyl-2-substituted-[1,4]-benzothiazin-3-one (P1 and P2) as corrosion inhibitors for mild steel in 1M HCl solution using weight loss, potentiodynamic polarization, electrochemical impedance spectroscopy (EIS) measurements and quantum chemical method. The structure of inhibitors is shown in Fig. 1.

Figure 1: Structures of the two benzothiazine derivatives, P1 (X : CH₂) and P2 (X : C=CH-C₆H₅).

2. Experimental

2.1. Inhibitors

• Synthesis and crystallization

To a solution of 2-substituted-[1,4]-benzothiazin-3-one (P1 and P2: 2 mmol), potassium carbonate (0.55 g, 4 mmol) and tetra n-butyl ammonium bromide (0.064 g, 0.2 mmol) in DMF (15 ml) was added 1-bromodecane (0.85 ml, 4 mmol). Stirring was continued at room temperature for 12 h. The mixture was filtered and the solvent removed. The residue was extracted with water. The organic compound was chromatographed on a column of silica gel with ethyl acetate-hexane (9/1) as eluent. Yellow oil were isolated when the solvent was allowed to evaporate (Figure 2).

Figure 2: Characterization of the benzothiazine derivatives, P1 and P2.

• Identification

The analytical and spectroscopic data are conforming to structures of compounds formed.

(P3): Yield: 41%; mp: Yellow oil; RMN¹H (DMSO-d₆) δ ppm: 6.98-7.47 (m, 4H, H_{arom}); 3.87 (t, 2H, N-CH₂-, J= 7.2Hz); 3.43 (s, 2H, SCH₂); 1.61 (m, 2H, N-C-CH₂); 1.21-1.23 (m, 14H, CH₂); 0.84 (t, 3H, -CH₃, J= 7.2Hz).

RMN¹³C (DMSO-d₆) δ ppm: 165.0 (C=O); 139.4, 123.6 (C_q); 128.4, 127.8, 123.4, 118.4 (CH_{arom}); 31.2, 31.1, 27.4, 27.2, 26.8, 26.6, 26.3, 22.4 (CH₂); 43.2 (NCH₂); 31.4 (S-CH₂); 14.3 (CH₃).

(P4): Yield: 65%; mp: brown oil; RMN¹H (DMSO-d₆) δ ppm: 7.73 (s, 1H, CH_{allyle}); 7.04-7.62 (m, 9H, H_{arom}); 4.03 (t, 2H, NCH₂-, J= 7.5Hz); 1.6 (m, 2H; N-C-CH₂); 1.24-1.26 (m, 14H, CH₂); 0.82 (t, 3H, -CH₃, J= 6.7Hz).

RMN¹³C (DMSO-d₆) δ ppm: 160.9 (C=O); 136.3, 134.2, 121.0, 118.6 (C_q); 134.2 (CH_{allyle}); 130.6, 129.5, 129.0, 128.0, 126.8, 124.1, 117.9 (CH_{arom}); 44.2 (NCH₂); 31.6, 29.4, 29.3, 29.2, 29.1, 27.0, 26.6, 22.4 (CH₂); 14.2 (CH₃).

2.2. Materials

Corrosion tests were performed using coupons prepared from steel having the composition: 0.09% P; 0.38% Si; 0.01% Al; 0.05% Mn; 0.21% C; 0.05% S and 99.21% Fe were polished with emery paper up to 1200 grade, washed thoroughly with double-distilled water, degreased with AR grade ethanol, acetone and dried at room temperature. Mild steel samples of size 1 × 1 × 0.1 cm and MS powder were used for weight loss studies. For electrochemical studies, specimens with an exposed area of 1 cm² were used. These specimens were degreased ultrasonically with 2-propanol and polished mechanically with different grades of emery paper to obtain very smooth surface.

1.3 Solution

The test solutions were prepared by the dilution of analytical grade 37 % HCl with distilled water up to the optimum inhibitor concentration of P1 and P2. For pH studies, the test solutions were prepared by the dilution of distilled water up to the optimum concentration, which was reached by adjusting the pH using HCl and NaOH. Inhibitor was dissolved in acid solution at required concentrations in (mol/L) and the solution in the absence of

inhibitor was taken as blank for comparison purposes. The test solutions were freshly prepared before each experiment by adding P1 and P2 directly to the corrosive solution. Experiments were conducted on several occasions to ensure reproducibility. Concentrations of P1 and P2 were 10^{-6} , 10^{-5} , 10^{-4} and 10^{-3} M.

1.4 Weight loss measurements

Gravimetric measurements were realized in a double walled glass cell equipped with a thermostat-cooling condenser. The mild steel sheets were abraded with a different grade of emery paper (120-400-600-1200) and then washed thoroughly with distilled water and acetone. After weighing accurately, the specimens were immersed in beakers which contained 100 mL acid solutions without and with various concentrations of P1 and P2 at temperature equal to 308 K remained by a water thermostat for 6h as immersion time. The gravimetric tests were performed by triplicate at same conditions. The corrosion rates (C_R) and the inhibition efficiency (η_{WL} %) of mild steel have been evaluated from mass loss measurement using the following equations:

$$C_R = \frac{W_b - W_a}{At} \quad (1)$$

$$\eta_{WL}(\%) = \left(1 - \frac{w_i}{w_0}\right) \times 100 \quad (2)$$

where W_b and W_a are the specimen weight before and after immersion in the tested solution, w_0 and w_i are the values of corrosion weight losses of mild steel in uninhibited and inhibited solutions, respectively, A the total area of the mild steel specimen (cm^2) and t is the exposure time (h).

2.5 Electrochemical measurements

The potentiodynamic polarization curves were conducted using an electrochemical measurement system PGZ 100 Potentiostat/Galvanostat controlled by a PC supported by the Voltmaster 4.0 Software. The electrochemical measurements were performed in a conventional three electrode glass cell with mild steel as a working electrode, platinum as counter electrode (Pt) and a saturated calomel electrode used as a reference electrode. The working electrode surface was prepared as described above gravimetric section. Prior to each electrochemical test an immersion time of 30 min was given to allow the stabilization system at corrosion potential. The polarization curves were obtained by changing the electrode potential automatically from -700 to -200 mV/SCE at a scan rate of 0.5 mV s^{-1} . The temperature is thermostatically controlled at desired temperature $\pm 1\text{K}$. The percentage protection efficiency η_{Tafel} (%) is defined as:

$$\eta_{Tafel}(\%) = \frac{I_{corr} - I_{corr(i)}}{I_{corr}} \times 100 \quad (3)$$

Where I_{corr} and $I_{corr(i)}$ are the corrosion current densities for steel electrode in the uninhibited and inhibited solutions, respectively.

Electrochemical impedance spectroscopy (EIS) measurements were carried out with same equipment used for potentiodynamic polarization study (Voltalab PGZ 100) at applied sinusoidal potential waves of 10 mV amplitudes with frequencies ranging from 100 KHz to 10 mHz at corrosion potential. The impedance diagrams are given in the Nyquist representation. The charge transfer resistance (R_{ct}) was determined from Nyquist plots and double layer capacitance (C_{dl}) was calculated from CPE parameters of the equivalent circuit deduced using Zview software. In this case the percentage protection efficiency (η_z %) is can be calculated by the value of the charge transfer resistance (R_{ct})

$$\eta_z\% = \frac{R_{ct}^i - R_{ct}^\circ}{R_{ct}^i} \times 100 \quad (4)$$

Where, R_{ct}° and R_{ct}^i are the charge transfer resistance in absence and in presence of inhibitor, respectively.

2.6. Quantum chemical calculations

Complete geometry optimization of the inhibitor molecules were performed using density functional theory (DFT) with Beck's three-parameter exchange functional along with Lee-Yang-Parr non-local correlation

functional (B3LYP) with 6-1G* basis set using the Gaussian 03 programme package [18]. Frontier molecular orbitals (HOMO and LUMO) were used to interpret the adsorption of inhibitor molecules on the metal surface. According to DFT Koopman's theorem [19,20], the ionization potential (I) is approximated as the negative of the highest occupied molecular orbital energy (E_{HOMO}) and the negative of the lowest unoccupied molecular orbital energy (E_{LUMO}) is related to the electron affinity (A).

$$I = - E_{HOMO} \quad (5)$$

$$A = - E_{LUMO} \quad (6)$$

Natural bond orbital (NBO) analysis was performed to evaluate the electron density distributions. The electrondensity plays an important role in calculating the chemical reactivity parameters. The global reactivities include electronegativity (χ), global hardness (η) and the global softness (σ). They can be calculated from the following equations:

$$\chi = \frac{I + A}{2} \quad (7)$$

$$\eta = \frac{I - A}{2} \quad (8)$$

$$\sigma = \frac{1}{\eta} = - \frac{2}{E_{HOMO} - E_{LUMO}} \quad (9)$$

The number of transferred electrons (ΔN) was also calculated depending on the quantum chemical method [21,22], by according the equation:

$$\Delta N = \frac{\chi_{Fe} - \chi_{inh}}{2(\eta_{Fe} + \eta_{inh})} \quad (10)$$

Where χ_{Fe} and χ_{inh} denote the absolute electronegativity of iron and inhibitor molecule η_{Fe} and η_{inh} denote the absolute hardness of iron and the inhibitor molecule respectively. In this study, we use the theoretical value of $\chi_{Fe} = 7.0$ eV and $\eta_{Fe} = 0$, for calculating the number of electron transferred.

2. Results and Discussion

3.1. Gravimetric measurements

The corrosion rate of mild steel specimens after exposure to 1M HCl solution with and without the addition of various concentrations of both inhibitors was calculated in $\text{mg cm}^{-2} \text{h}^{-1}$ and the data obtained are given in Table 1. The inhibition efficiencies ($\eta_{WL}\%$) were calculated and the data obtained given in the same Table 1. It can be seen from Table 1 that, the addition of P1 and P2 to the aggressive solution reduces the corrosion rate of mild steel (Fig. 3). The corrosion rate decreased and inhibition efficiency increased with increasing inhibitors concentration (Fig. 4) suggests that the inhibitors molecules act by adsorption on the metal surface [23].

Table 1: Weight loss values of various concentrations of P1 and P2 in 1M HCl solution at 308 K.

Medium	Conc (M)	C_R ($\text{mg}/\text{cm}^2 \text{h}$)	θ	η_{WL} (%)
HCl	1	0.7561	—	—
P1	10^{-3}	0.0175	0.977	97.7
	10^{-4}	0.1194	0.842	84.2
	10^{-5}	0.1442	0.809	80.9
	10^{-6}	0.2187	0.711	71.1
P2	10^{-3}	0.0360	0.952	95.2
	10^{-4}	0.1307	0.827	82.7
	10^{-5}	0.1745	0.769	76.9
	10^{-6}	0.2278	0.699	69.9

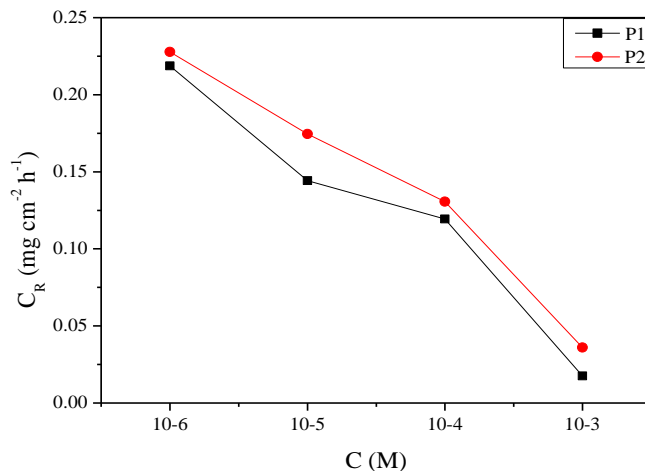


Figure 3: Relationship between corrosion rate (C_R) and concentration of P1 and P2 in 1M HCl at 308 K.

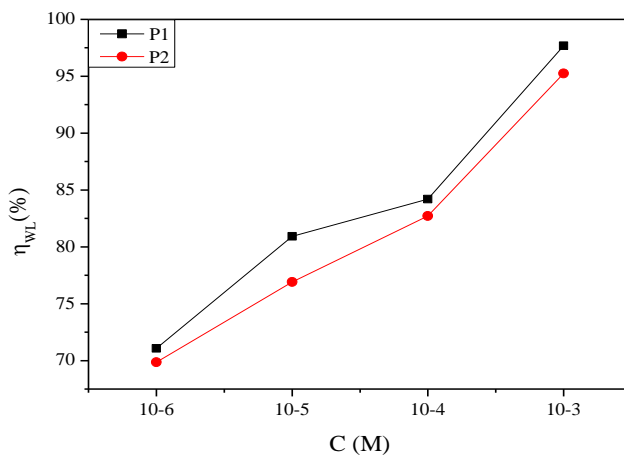


Figure 4: Relationship between inhibition efficiency (η_{WL} %) and P1 and P2 in 1M HCl at 308 K.

3.2. Polarization potentiodynamic results

The polarization curves of mild steel in HCl medium in the presence and absence of inhibitors are shown in Figs. 5a and 5b. It is shown that when the concentration of inhibitors increases, there is a change in the corrosion rate to lower values and efficacy of inhibition due to the action of inhibitors.

Electrochemical corrosion kinetics parameters such as corrosion potential (E_{corr}), cathodic and anodic Tafel slope (β_c , β_a), the inhibition efficiency (η_{Tafel} %) and corrosion current density (I_{corr}) were given in Table 2.

Analysis on the polarization curves show that in the presence of the inhibitors, the cathodic and anodic curves were slightly shifted. An inhibitor can be classified as cathodic or anodic type if the displacement in corrosion potential is more than 85 mV with respect to corrosion potential of the blank [24]. This indicates that P1 and P2 act as a mixed type inhibitors. Note the suppression of the two anodic and cathodic reactions of the corrosion of mild steel in a hydrochloric acid solution, and when the concentration of inhibitor P1 and P2 increases, the inhibitory efficiency increases. It is known that when the E_{corr} shifts slightly, the inhibitor act as mixed type inhibitor [25]. In addition, cathodic current-potential curves give rise to parallel Tafel lines, which indicates that the addition of inhibitors does not modify the mechanism of the reaction [26]. The results demonstrate that the inhibition efficiency increases with inhibitors concentration. It also can be seen from Table 2 that the corrosion current density decreases with incremental inhibitor concentration, and this decrease is more pronounced in the case of P1. Thus, P1 exhibits higher inhibitive efficiency than P2.

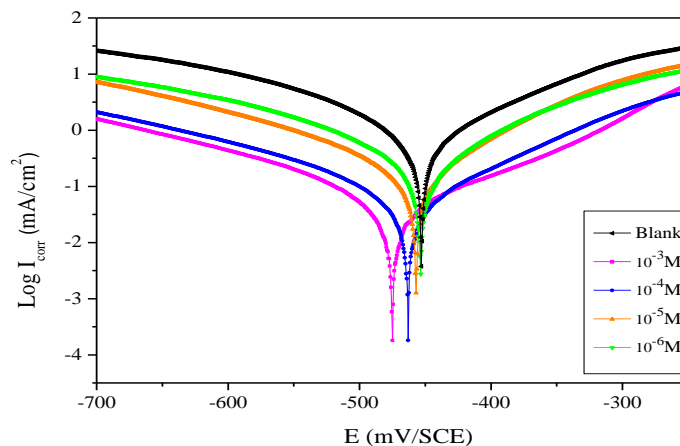


Figure 5a: Polarisation curves of mild steel in 1M HCl for various concentrations of P1 at 308K.

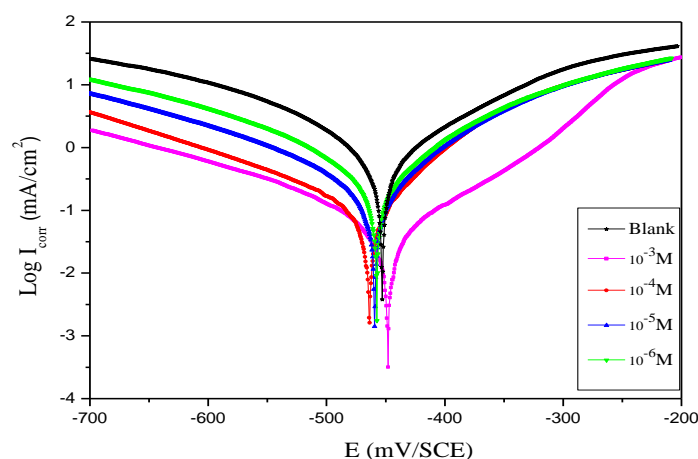


Figure 5b: Polarisation curves of mild steel in 1M HCl for various concentrations of P2 at 308K.

Table 2: Polarization data of mild steel in 1M HCl without and with addition of inhibitors at 308 K.

Medium	Conc (M)	$-E_{\text{corr}}$ (mV/SCE)	I_{corr} ($\mu\text{A}/\text{cm}^2$)	$-\beta_c$ (mv/dec)	β_a (mv/dec)	η_{Tafel} (%)
HCl	1	453	1560	174	145	—
P1	10^{-3}	475	95	184	114	93.9
	10^{-4}	463	115	186	128	92.6
	10^{-5}	457	303	169	109	80.6
	10^{-6}	453	744	217	163	52.3
P2	10^{-3}	448	105	199	95	93.3
	10^{-4}	463	139	165	74	91.1
	10^{-5}	459	395	186	110	74.7
	10^{-6}	457	808	198	146	48.2

3.3. Electrochemical impedance spectroscopy

Figs. 6a and 6b show the representative Nyquist plots of mild steel obtained in 1M HCl solution in the absence and presence of various concentrations of inhibitors studied (P1 and P2). The electrochemical parameters derived from the Nyquist plots are given in Table 3.

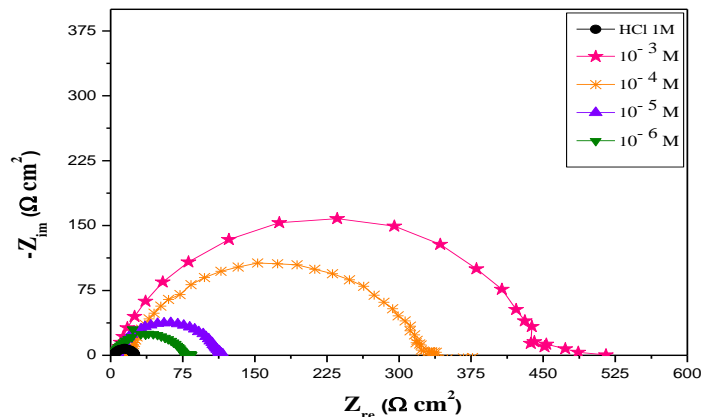


Figure 6a: Nyquist curves for mild steel in 1M HCl for selected concentrations of P1 at 308 K.

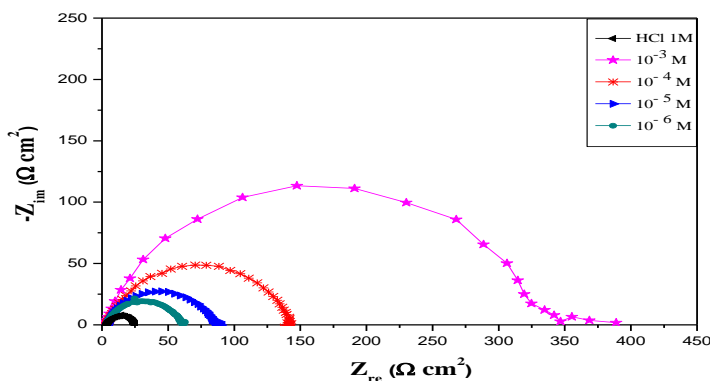


Figure 6b: Nyquist curves for mild steel in 1M HCl for selected concentrations of P2 at 308K.

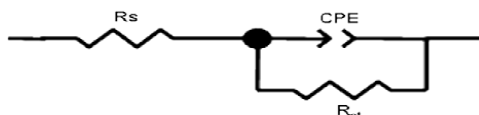


Figure 7: Equivalent electrical circuit model

The Nyquist diagrams show a single semicircle shifted along the real impedance axis (Z_{real}), indicating that the corrosion of mild steel in 1M HCl is controlled by a charge-transfer process [27]. For analysis of the impedance spectra containing a single capacitive semicircle, the standard Randle's circuit is used [28] (Fig. 7), where the circuit is composed of a solution resistance component (R_s) and a capacitance component (C_{dl}). The resistor R_s is in series to the double layer capacitance and R_{ct} while double layer capacitance is parallel to R_{ct} . Similar figures have been described in literature for the acidic corrosion of iron and mild steel in the presence and absence of various inhibitor molecules [29,30]. The charge-transfer resistance values (R_{ct}) were obtained from the Z_{real} . The higher-frequency intersection corresponds to the solution resistance (R_s), and the lower-frequency intersection corresponds to $R_s + R_{ct}$. Thus, R_{ct} values were calculated as the difference between the high- and low-frequency intersection values [31]. Double-layer capacitance (C_{dl}) values were calculated using the following equation [32]:

$$C_{dl} = \frac{1}{2\pi f_{max} R_{ct}} \quad (11)$$

Where f_{max} is the frequency value at which the imaginary component of the impedance is greatest.

The semicircle corresponds to a capacitive loop in the obtained electrochemical impedance diagrams. Deviations from a perfectly circular shape indicate the frequency dispersion of the interfacial impedance [33]. The diameter

of the capacitive loop increased in the presence of the inhibitors. Table 3 shows that the R_{ct} values increased and the C_{dl} values decreased with increasing inhibitor concentration.

The increase in R_{ct} value can be attributed to the formation of protective film on the metal/solution interface. The decrease in the C_{dl} values may be caused by a decrease in the local dielectric constant and/or an increase in the thickness of the electrical double layer, indicating that the inhibitors function by adsorption at the metal surface [34,35]. The sequence of the inhibitors efficiencies were following the order of $P1 > P2$ which is in agreement with the results obtained from the polarization technique.

Table 3: EIS parameters for the corrosion of mild steel in 1M HCl containing P1 and P2 at 308 K.

Medium	Conc (M)	R_{ct} ($\Omega \text{ cm}^2$)	C_{dl} ($\mu\text{F}/\text{cm}^2$)	η_z (%)
HCl	1	25	148	—
P1	10^{-3}	448	36	94.4
	10^{-4}	331	40	92.4
	10^{-5}	114	87	78.1
	10^{-6}	76	92	67.1
P2	10^{-3}	338	46	92.6
	10^{-4}	142	47	82.4
	10^{-5}	86	96	70.9
	10^{-6}	61	110	59.0

3.4. Adsorption isotherm and thermodynamic parameters

Basic information on the interaction between an organic inhibitor and a mild steel surface can be obtained from various adsorption isotherms. The most commonly used adsorption isotherms are the Langmuir, Temkin, and Frumkin isotherms. The surface coverage (θ) [$\eta_{WL} \% = 100 \times \theta$] for different concentrations of inhibitor in 1M hydrochloric acid was tested graphically to determine a suitable adsorption isotherm.

Plots of C/θ versus C yielded straight lines (Figure 8) with correlation coefficient (R^2) values of 0.99966 and 0.99970 for P1 and P2, respectively, at 308 K.

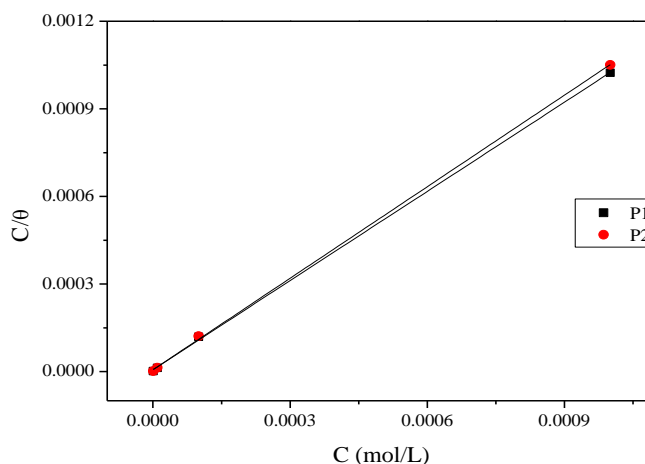


Figure 8: Langmuir adsorption isotherm for mild steel immersed in 1M HCl solution in presence of various concentrations of P1 and P2.

This indicates that the adsorption of these inhibitors can be fitted to the Langmuir adsorption isotherm, represented by the equation:

$$\frac{C}{\theta} = \frac{1}{K_{ads}} + C \quad (12)$$

θ is the surface coverage, K_{ads} is the adsorption-desorption equilibrium constant, C is the concentration of inhibitor. From the intercepts of the straight lines on the C/θ axis, K_{ads} values were calculated for the adsorption process (Table 4). Free energy of adsorption (ΔG_{ads}°) was calculated by using following equation Eq. (13),

$$\Delta G_{ads}^{\circ} = -RT \ln(55.5 K_{ads}) \quad (13)$$

where R is gas constant and T is absolute temperature of experiment and the constant value of 55.5 is the concentration of water in solution in mol L⁻¹.

Table 4: Thermodynamic parameters for the adsorption of inhibitors in 1M HCl on mild steel at different concentrations

Inhibitors	R ²	Slopes	K _{ads} (L/mol)	ΔG_{ads}° (kJ/mol)
P1	0.99966	1.02	162549.03	-41.01
P2	0.99970	1.04	163579.91	-41.03

Results presented in the Table 4, indicate that the values of ΔG_{ads}° are negative. The negative values signify adsorption of the inhibitor molecules via mixed adsorption mechanism. Literature demonstrates that the values of standard Gibbs free energy of adsorption in aqueous solution around -20 kJ mol⁻¹ or lower (more positive) indicate adsorption with electrostatic interaction between the adsorbent and adsorbate (physisorption), while those around or higher (more negative) than -40 kJ mol⁻¹ involve charge sharing between the molecules and the metal (chemisorption) [36]. However, this should be taken with caution since the enthalpy of adsorption is the parameter that actually reflects the adsorption bond strength, rather than the standard Gibbs free energy of adsorption [37]. Physisorption is consistent with electrostatic interaction between charged molecules and a charged mild steel surface while chemisorption is consistent with charge sharing or charge transfer from the inhibitor components to the metal surface to form a coordinate type of bond. Calculated ΔG_{ads}° values indicated that the adsorption mechanism of the prepared compounds on mild steel in 1M HCl solution is a chemical adsorption [38].

3.6. Quantum chemical studies

The aim of quantum chemical calculation is to evaluate the inhibition performance of corrosion inhibitors, which can quantitatively study the relationship between inhibition efficiency and molecular reactivity [39], so we can predicted the capability of inhibitor molecules to donate or accept electrons by analysis of global reactivity parameters, such as the energy gap between HOMO and LUMO, chemical hardness, and dipole moment.

E_{HOMO} indicates the tendency of an organic molecule to donate electrons. The higher the value of E_{HOMO} , the greater the ability of a molecule to donate electrons while E_{LUMO} indicates the propensity of a molecule to accept electrons. The lower E_{LUMO} is the greater ability of that molecule to accept electrons. Thus, the binding ability of organics to the metal surface increases with an increase in energy of the HOMO and a decrease in the value of energy of the LUMO. The energy gap, ΔE , is an important parameter which indicates the reactivity tendency of organics toward the metal surface [40]. As ΔE decreases, the reactivity of the molecule increases, leading to an increase in adsorption onto a metal surface. A molecule with low energy gap is more polarizable and is generally associated with high chemical reactivity and low kinetic stability. Thus, ΔE has been used in literature to characterize the binding ability of organics to the metal surface [41].

Figure 9 shows the optimized geometry, the HOMO density distribution and the LUMO density distribution of studied molecules (P1 and P2) by B3LYP/6-31G(d,p) method. The calculated quantum chemical parameters of the two inhibitors are shown in Table 5. The energy of HOMO (E_{HOMO}) is related to the electron donating capacity of the molecule and the values indicate that the molecule has a tendency to donate orbital electrons to appropriate acceptor molecules with low energy or empty the 3-d orbital of Fe to form a coordinate bond [41,42]. It is well established that the higher the HOMO energy of the inhibitor, the greater is its tendency to donate electrons to unoccupied d orbital of the metal, and the higher will be the corrosion inhibition efficiency [43]. The energy of HOMO measures the tendency towards the donation of electrons by the molecule.

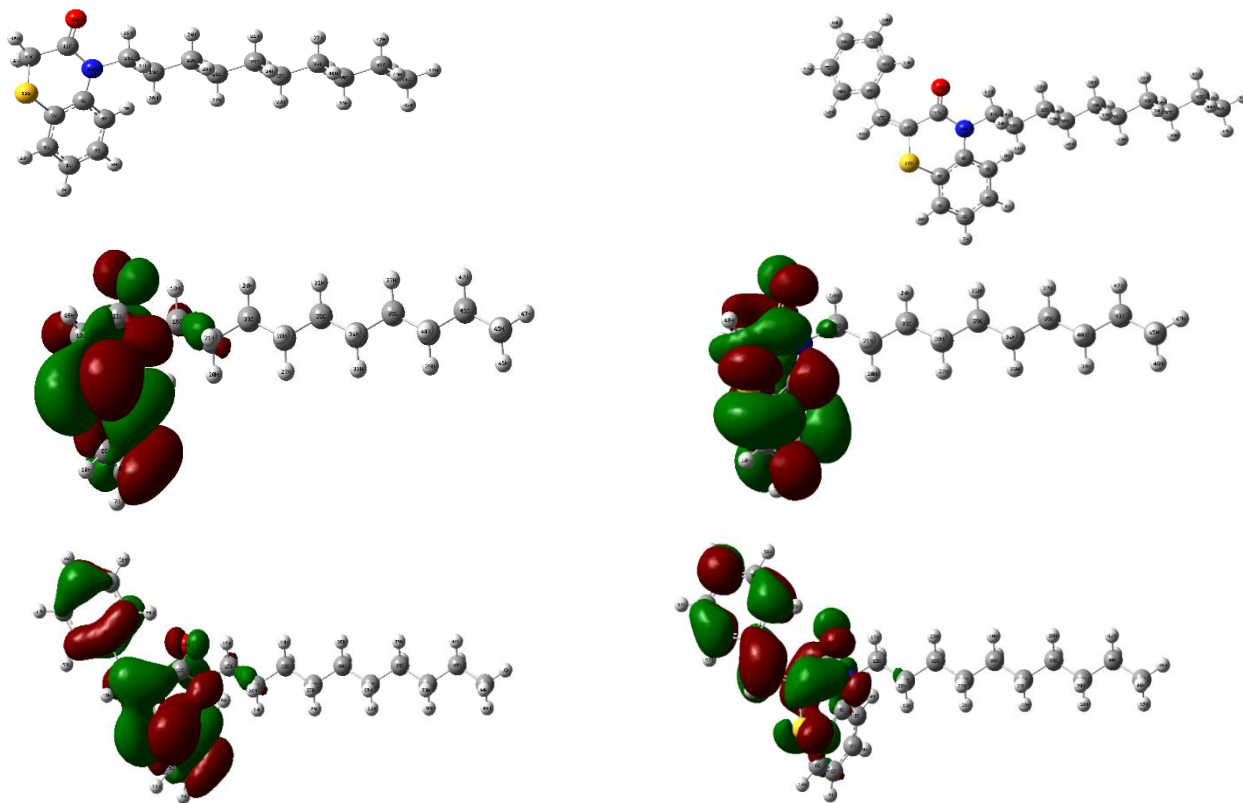


Figure 9: The frontier molecule orbital density distributions of P1 and P2: HOMO (left) and LUMO (right).

The energy of LUMO indicates the ability of a molecule to accept electrons. Lower the values of E_{LUMO} , the more probable is the molecule to accept electrons. The inhibitor not only donates electrons to the unoccupied d-orbital of the metal ion, but can also accept electrons from the d-orbital of the metal leading to the formation of a feedback bond [44]. From Table 5, E_{HOMO} obeys the order: $P1 > P2$. Obviously, this sequence is in completely accordance with the order of inhibition efficiency. This may explain the better inhibition efficiency of P1 molecule than P2 is due to the higher E_{HOMO} . On the other hand, E_{LUMO} obeys the order: $P2 > P1$, which is not agreement with the sequence of inhibition efficiency. The separation energy (ΔE) is an important parameter as a function of reactivity of the inhibitor molecule toward the adsorption on metallic surface. As ΔE decreases, the reactivity of the molecule increases in visa, which facilitates adsorption and enhances the efficiency of inhibitor [22]. Inspection of the data in Table 5 reveals ΔE obeys the order of $P2 < P1$, which is in completely accordance with the order of inhibition efficiency of $P2 > P1$. Thus, there is a good correlation between ΔE and inhibition efficiency.

The dipole moment (μ) is another important electronic parameter, used for the prediction of the direction of a corrosion inhibition process. The dipole moment gives information on the polarity (hydrophobicity) in a bond of a molecule and therefore the electron distribution in the molecule [45,46]. It is generally agreed that the adsorption of high polar compounds possessing high dipole moment on the metal surface should lead to better inhibition. In our study the dipole moment of the P1 compound is 2.9553 D and P2 compound is 2.5379 D. The high value of the dipole moment of the P1 inhibitor shows higher inhibition efficiency.

According to some published papers [47], the parameter of χ is related to the chemical potential, and higher χ means better inhibitive performance. On the other hand, η is equal to $\Delta E/2$, and the lower η implies more polarizability and higher inhibition efficiency. The parameter of σ is reciprocal to η , thus high value of σ is related to more efficiency. Values of ΔN exhibit inhibitive performance resulted from electrons donations. If $\Delta N < 3.6$, the inhibition performance increases with the increase in electron-donation ability to the metal surface

[47]. In the present study, inhibition efficiency follows the order: P1 > P2. Thus, there is not a good correlation between inhibitive performance and the parameters of η and ΔN .

Table 5: Quantum chemical parameters for P1 and P2.

Quantum parameters	P1	P2
E_{HOMO} (eV)	-5.8548	-5.6463
E_{LUMO} (eV)	-0.7270	-1.5034
ΔE gap (eV)	5.1278	4.1429
μ (debye)	2.9553	2.5379
$I = -E_{HOMO}$ (eV)	5.8548	5.6463
$A = -E_{LUMO}$ (eV)	0.7270	1.5034
$\chi = \frac{I + A}{2}$ (eV)	3.2909	3.57485
$\eta = \frac{I - A}{2}$ (eV)	2.5639	2.07145
$\sigma = \frac{1}{\eta}$	0.39003	0.48275
$\Delta N = \frac{\chi_{Fe} - \chi_{inh}}{2(\eta_{Fe} + \eta_{inh})}$	0.72333	0.82675

Conclusion

Two benzothiazine derivatives of 4-decyl-2H-benzo[b][1,4]thiazin-3(4H)-one (P1) and 2-benzylidene-4-decyl-2H-benzo[b][1,4]thiazin-3(4H)-one (P2) are good inhibitors for the corrosion of mild steel in 1M HCl solution. Inhibition efficiency increases with increase in the concentration of each inhibitor, the maximum values of inhibition efficiency reach until 97.7%. The adsorption of P1 or P2 obeys Langmuir adsorption isotherm. Both benzothiazine derivatives act as mixed-type inhibitors. EIS spectra exhibit individual capacitive loop. The presence of inhibitor in 1M HCl solutions increases R_{ct} while reduces C_{dl} . There is a good correlation between inhibition efficiency and the quantum parameters of E_{HOMO} , ΔE and μ . The inhibition ability of the two benzothiazine compounds follows the order: P1 > P2, which has been confirmed by the weight loss, electrochemical measurements and theoretical calculation measurements.

References

- Schmitt G., *Brit. Corros. J.* 19 (1984) 165.
- Zhang Q. B., Hua Y. X., *Electrochim. Acta* 54 (2009) 1881.
- Zarrok H., Oudda H., El Midaoui A., Zarrouk A., Hammouti B., Ebn Touhami M., Attayibat A., Radi S., Touzani R., *Res. Chem. Intermed.*, 38 (2012) 2051.
- Zarrouk A., Hammouti B., Zarrok H., Bouachrine M., Khaled K.F., Al-Deyab S.S., *Int. J. Electrochem. Sci.*, 6 (2012) 89.
- Zarrouk A., Hammouti B., Dafali A., Zarrok H., *Der Pharm. Chem.*, 3 (2011) 266.
- Zarrok H., Zarrouk A., Salghi R., Oudda H., Hammouti B., Assouag M., Taleb M., Ebn Touhami M., Bouachrine M., Boukhris S., *J. Chem. Pharm. Res.*, 4 (2012) 5056.
- Ghazoui A., Zarrouk A., Bencat N., Salghi R., Assouag M., El Hezzat M., Guenbour A., Hammouti B., *J. Chem. Pharm. Res.*, 6 (2014) 704.
- Zarrok H., Zarrouk A., Salghi R., Assouag M., Hammouti B., Oudda H., Boukhris S., Al Deyab S.S., Warad I., *Der Pharm. Lett.*, 5 (2013) 43.
- Dafali A., Hammouti B., Mokhlisse R., Kertit S., Elkacemi K., *Corros. Sci.* 45 N°8 (2003) 1619.
- Hammouti B., Dafali A., Touzani R., Bouachrine M., *Journal of Saudi Chemical Society*, 16 N°4 (2012) 413.

11. Wang L., *Corros. Sci.*, 48 (2006) 608.
12. Elyoussfi A., Dafali A., Elmsellem H., Steli H., Bouzian Y., Cherrak K., El Ouadi Y., Zarrouk A., Hammouti B., *J. Mater. Environ. Sci.* 7 (9) (2016) 3344.
13. Obot I.B., Obi-Egbedi N.O., *Corros. Sci.* 52 (2010) 657.
14. Wang D., Li S., Ying Y., Wang M., Xiao H., Chen Z., *Corros. Sci.* 41 (1999) 1911.
15. Donnelly B., Downie T.C., Grzeskowiak R., Hamburg H.R., Short D., *Corros. Sci.* 18 (1977) 109.
16. Obot I.B., Obi-Egbedi N.O., Umoren S.A., *Corros. Sci.*, 51 (2009) 276.
17. Dafali A., Hammouti B., Touzani R., Kertit S., Ramdani A., Elkacemi K., *Anti-corros. Meth. & Mat.*, 49N°2 (2002) 96.
18. Gaussian 03, Revision B.01, M. J. Frisch, et al., *Gaussian, Inc., Pittsburgh, PA*, 2003.
19. Hehre W.J., Radom L., Schleyer P.v.R., Pople A.J., *Wiley-Interscience, New York*, 1986.
20. Janak J.F., *Phys. Rev. B* 18 (1978) 7165.
21. Sastri V.S., Perumareddi J.R., *Corrosion (NACE)* 53 (1997) 617.
22. Lukovits I., Kalman E., Zucchi F., *Corrosion (NACE)*, 57 (2001) 3.
23. Zarrouk A., Warad I., Hammouti B., Dafali A., Al-Deyab S.S., Benchat N., *Int. J. Electrochem. Sci.*, 5(10) (2010) 1516.
24. Verma C., Quraishi M.A., Singh A., *J. Mol. Liq.*, 212 (2015) 804.
25. Verma C.B., Ebenso E.E., Bahadur I., Obot I.B., Quraishi M.A., *J. Mol. Liq.*, 212 (2015) 209.
26. Benabdellah M., Touzani R., Aouniti A., Dafali A., El Kadiri S., Hammouti B., Benkaddour M., *Mater. Chem. Phys.* 105 (2-3) (2007) 373.
27. Khaled K.F., *Appl. Surf. Sci.* 255 (2008) 1811.
28. Achary G., Sachin H.P., Naik A., Venkatesha T.V., *Mater. Chem. Phys.*, 107 (2008) 44.
29. Ashassi-Sorkhabi H., Shaabani B., Seifzadeh D., *Appl. Surf. Sci.* 239 (2005) 154.
30. Bouklah M., Hammouti B., Benkaddour M., Benhadda T., *J. Appl. Electrochem.*, 35 (2005) 1095.
31. Emregul K.C., Duzgun E., Atakol O., *Corros. Sci.* 48 (2006) 3243.
32. Tebbji K., Faska N., Tounsi A., Oudda H., Benkaddour M., Hammouti B., *Mater. Chem. Phys.* 106 (2007) 260.
33. El Ouasif L., Merini I., Zarrok H., El ghouli M., Achour R., Guenbour A., Oudda H., El-Hajjaji F., Hammouti B., *J. Mater. Environ. Sci.* 7 (8) (2016) 2718-2730
34. Prabhu R.A., Venkatesha T.V., Shanbhag A.V., Kulkarni G.M., Kalkhambkar R.G., *Corros. Sci.*, 50 (2008) 3356.
35. Tang Y., Yang X., Yang W., Chen Y., Wan R., *Corros. Sci.*, 52 (2010) 242.
36. Bilgic S., Sahin M., *Mater. Chem. Phys.*, (2001) 290.
37. Gharebaa S., Omanovic S., *Corros. Sci.*, 52 (2010) 2104.
38. Behpour M., Ghoreishi S.M., Soltani N., Salavati-Niasari M., Hamadani M., Gandomi A., *Corros. Sci.*, 50 (2008) 2172.
39. Belghiti M.E., Karzazi Y., Tighadouini S., Dafali A., Jama C., Warad I., Hammouti B., Radi S., *J. Mater. Environ. Sci.* 7 (3) (2016) 956.
40. Aytac A., Bilgic S., Gece G., Ancin N., Oztas S.G., *Mater. Corros.*, 63(8) (2012) 729.
41. Ahamad I., Prasad R., Quraishi M.A., *Corros. Sci.*, 52 (2010) 1472.
42. Fang J., Li J., *J. Mol. Struct.*, 593 (2002) 179-185.
43. Singh A.K., Khan S., Singh A., Quraishi S.M., Quraishi M.A., Ebenso E.E., *Res. Chem. Intermed.* 39 (2013) 1191.
44. Sudheer, Quraishi M.A., *Corros. Sci.*, 70 (2013) 161.
45. Ebenso E.E., Isabiye D.A., Eddy N.O., *Int. J. Mol. Sci.*, 11 (2010) 2473.
46. Gece G., *Corros. Sci.*, 50 (2008) 2981.
47. Al Mamari K., Elmsellem H., Sebbar N. K., Elyoussfi A., Steli H., Ellouz M., Ouzidan Y., Nadeem A., Essassi E. M., El-Hajjaji F., *J. Mater. Environ. Sci.* 7 (9) (2016) 3286-3299

(2017) ; <http://www.jmaterenvionsci.com/>